The Astronomical Journal, 166:170 (9pp), 2023 October https://doi.org/10.3847/1538-3881/acf7c8

Revisiting Galactic Disk and Spiral Arms Using Open Clusters

Yogesh C. Joshi[1] and Sagar Malhotra[2]
[1] Aryabhatta Research Institute of Observational Sciences (ARIES), Manora Peak, Nainital 263002, India; yogesh@aries.res.in
[2] Indian Institute of Science Education & Research, Mohali 140306, India
Received 2023 August 5; revised 2023 August 31; accepted 2023 September 6; published 2023 September 22

Abstract

We use the largest catalog of open clusters in the post-Gaia era to provide an observational view of the Galactic disk. By compiling physical parameters such as age, distance, and kinematic information, we investigate the spatial distribution of open clusters and revisit the spiral arms and other asymmetries in the Galactic disk. Using young open clusters as a tracer of spiral arms, we map the spiral structure of the Galaxy and find that most of the clusters start migrating away from the spiral arms in about 10–20 Myr and fill the interarm regions as they age. Using the 3D kinematic information on 371 open star clusters, we derive different individual pattern speeds for spiral arms that closely follow the rotation curve of the Milky Way, hence favoring the transient nature of spiral arms in the Milky Way. The pattern rotation speeds of each spiral arm suggest that the spiral arms have not accelerated in the last 80 Myr. Based on the distribution of open clusters younger than 700 Myr above or below the Galactic plane, we found a solar offset of $z_{\odot} = 17.0 \pm 0.9$ pc north of the Galactic plane and estimated the scale height $z_h = 91.7 \pm 1.9$ pc from the Galactic plane.

Unified Astronomy Thesaurus concepts: Galaxy structure (622); Milky Way disk (1050); Open star clusters (1160)

1. Introduction

Open star clusters (OCs) are a group of coeval stars that are formed as a clump in giant molecular clouds and provide vital clues to understanding star formation and evolution in the Galaxy (Portegies Zwart et al. 2010; Krumholz et al. 2019). As most OCs are relatively younger populations and lie mainly within the Galactic disk, these sources are being viewed as excellent markers to study the structural, kinematic, and chemical properties of the Galactic disk through analysis of a large number of clusters in the Galaxy. Many authors have carried out such studies in the past (see Bonatto et al. 2006; Buckner & Froebrich 2014; Joshi et al. 2016; Cantat-Gaudin et al. 2020; Dobbs et al. 2022). Moreover, the wide range of ages of OCs, from a few million years to nearly 10 billion years, provides a unique opportunity to study the evolution of the Galactic disk and trace the star formation history across the Milky Way. In recent years, the number of OCs has grown manyfold (Cantat-Gaudin 2022; Castro-Ginard et al. 2022; Chi et al. 2023), paving the way for a better understanding of the Galactic disk, thanks to large-scale surveys and machine-learning methods (Cantat-Gaudin et al. 2018, 2019; Ryu & Lee 2018; Sim et al. 2019; Liu & Pang 2019; Dias et al. 2021; He et al. 2021; Hao et al. 2022b; Castro-Ginard et al. 2022). Accurate physical parameters for OCs are obtained through analysis of precise membership identification of cluster stars facilitated through their astrometric and kinematic study (Dias et al. 2014, 2021; Cantat-Gaudin et al. 2018; Castro-Ginard et al. 2022; Zhong et al. 2022). It is important to note that much of this progress has come from the Gaia survey data, which provide unprecedented homogeneous and precise photometry, high-precision proper motion, and parallaxes of more than a billion sources (Gaia Collaboration et al. 2016, 2018), thereby leading to more precise and accurate estimation of the astrometric and physical parameters of OCs as compared to some pre-Gaia catalogs such as Dias et al. (2002) and Kharchenko et al. (2013).

Although substantial progress has been made in the past decade to understand the Galactic disk, it is still unclear exactly what mechanism drives the formation of spiral arms in the Galaxy, leading to a lack of consensus among the community on the nature of spiral arms. In the present study, we aim to use the catalog of largest open clusters compiled in the post-Gaia era to provide an observational view of the Galactic disk. This paper is organized as follows: we describe the data used in the present study in Section 2. The spatial distribution of the clusters in the Galaxy and spiral-arm morphology and kinematics are described in Section 3. Section 4 discusses the OC distribution along and perpendicular to the Galactic plane. The summary of our results is laid out in Section 5.

2. Data

We compiled a large catalog of OCs from more than 35 previous studies that provided their mean astrometric and physical parameters, including their age and distance. The list of references used in compiling the catalog, along with the corresponding number of OCs analyzed in each study, is provided in Table 1. The priority order of the references while compiling the catalog was decided by their year of publication and the Gaia data release used for studying OCs. Furthermore, since several clusters detected in the pre-Gaia era were found to be false positives when reinvestigated in the Gaia data (e.g., Cantat-Gaudin & Anders 2020), we have only included those OCs that have been discovered or revisited in the Gaia era. While prioritizing the latest studies and giving lesser weight to those showing multiple discrepancies, we compiled a catalog of 6133 OCs having information about positions, parallax, age, heliocentric distance, proper motions, and radial velocities, though not all the parameters are available for all the clusters. We preferred the cluster parameters from post-Gaia catalogs and only resorted to the pre-Gaia studies if no information was

Table 1
References Used to Compile the Catalog of 6133 OCs

Reference	No. of OCs	Reference	No. of OCs
Hao et al. (2022b)	704	Cantat-Gaudin & Anders (2020)	1481
Hao et al. (2022a)	38	Ferreira et al. (2020)	59
Castro-Ginard et al. (2022)	628	Bossini et al. (2019)	269
He et al. (2022a)	541	Ferreira et al. (2019)	4
He et al. (2022b)	886	Carrera et al. (2019)	90
Tarricq et al. (2022)	389	Cantat-Gaudin et al. (2018)	1229
Myers et al. (2022)	150	Donor et al. (2018)	19
Netopil et al. (2022)	136	Netopil et al. (2016)	172
Dias et al. (2021)	1743	Scholz et al. (2015)	63
Tarricq et al. (2021)	393[a]	Schmeja et al. (2014)	139
Hao et al. (2021)	3794	Kharchenko et al. (2013)	3006
Spina et al. (2021)	226	Buckner & Froebrich (2013)	775
Hu et al. (2021)	265	Vande Putte et al. (2010)	481
Casamiquela et al. (2021)	47	Glushkova et al. (2010)	194
Cantat-Gaudin et al. (2020)	2017	Mermilliod et al. (2008)	166
Donor et al. (2020)	128	Kharchenko et al. (2007)	516
Poovelil et al. (2020)	34[a]	Chen et al. (2003)	144
Kounkel et al. (2020)	1910	Dias et al. (2002)	2167
Zhong et al. (2020)	295	Loktin & Beshenov (2003)	347[b]

Notes. In some cases (footnotes a and b), we have considered only a subset of a given sample.
[a] High-quality sample.
[b] Reliable proper motions.

found in recent studies. Therefore, the final value of any parameter was the one provided in the most recent version of the catalog. Of the 6133 OCs in the catalog, all have their age estimates available, but only 4378 clusters have distance information. Among them, 2959 OCs have distance estimates from the Gaia data while the remaining 1419 OCs have distances retrieved from pre-Gaia era studies. Using the distance information, we estimated Cartesian coordinates (X, Y, Z) and the Galactocentric distance R_{GC} for all the 4378 OCs. In addition to this, the full 3D kinematic information is also available for 2483 OCs. Here, one has to note that since there are very few catalogs that provide the uncertainties in the estimated physical parameters of OCs, especially the distance, we have not used the distance uncertainties in our analysis.

3. Spatial Distribution

3.1. 2D Distribution of OCs and Present-day Spiral Arms

Knowledge of the spatial distribution of OCs is important for understanding the inhomogeneous nature of the Galaxy and probing the large-scale Galactic structure. For this purpose, we took advantage of the positional coordinates of all the 6133 OCs to infer the broader picture of the structure of the Milky Way. In Figure 1, we use mw-plot[3] to show an on-sky view of the Galaxy in the Galactic longitude–latitude (l–b) plane with OCs juxtaposed in the l–b plane wherein the image in the background is generated by ESA Gaia EDR3 and has a resolution of 15.38 lt-yr per pixel. It is evident that there are a few pockets where cluster density is low, such as in the regions of 50° and 150° Galactic longitude. The lack of OCs in a region near $l \sim 150°$ might be due to the lower density of gas and dust in the anticenter direction; this has also been noticed previously and dubbed the Gulf of Camelopardalis (Cantat-Gaudin et al. 2019; Castro-Ginard et al. 2019). The deficiency of clusters around the $l \sim 50°$ region might be understood as due to the higher disruption rate complemented by our obscured view in the direction of the Galactic center. The distribution of clusters is more scattered around the Galactic midplane toward the Galactic anticenter direction than in the direction of the Galactic center. However, in general, most of the clusters are confined very close to the Galactic midplane, and their number density decreases sharply as one goes away from the midplane, with more than 85% of the total number of OCs in the range [−10°, 10°] of Galactic latitude while 75% of them belong to the central [−5°, 5°] region.

To better resolve the multiple structures at various distances which are otherwise superposed on the sky, we illustrate the X–Y distribution of OCs in the left panel of Figure 2 with the Sun at (−8.15, 0) kpc (Reid et al. 2019) and the Galactic center at the origin. Here, we draw only the 4378 OCs for which distance information was available. The OCs detected far from the Galactic center are not shown in this plot for better visualization. OCs older than 700 Myr are shown in gray while the younger ones are colored according to their ages. We overplotted the usual log-periodic spiral arms taken from Hou (2021) where the profile of each arm is described by Reid et al. (2019) as follows:

$$\ln(R/R_{\rm kink}) = -(\beta - \beta_{\rm kink})\tan\psi$$

where R is the Galactic radius at a Galactocentric azimuth angle β, which is 0 along the line joining the Sun and the Galactic center and increases in the direction of Galactic rotation. $R_{\rm kink}$ and $\beta_{\rm kink}$ are the corresponding values of R and β at the kink position, where there might be an abrupt change in the pitch angle ψ. There has been substantial evidence in the recent past that spiral arms in our Galaxy as well as other galaxies are made up of small segments having a scale length of about 5–8 kpc that are separated by kinks/gaps (Honig & Reid 2015). A similar observation was made in N-body simulations by D'Onghia et al. (2013). Recent studies by Reid et al. (2019) and Hou (2021) use accurate measurements from very long baseline interferometry of parallaxes of masers etc. to fit log-periodic spiral arms while allowing for kinks resulting in improved quality of fits. This model of allowing kinks in the spiral arms is supported by several studies (e.g., Kendall et al. 2011; Honig & Reid 2015; Díaz-García et al. 2019) and found that spiral arms in different galaxies were not perfectly described by log-periodic spirals but rather were separated by gaps/kinks. Similarly, other studies (e.g., Taylor & Cordes 1993; Hou & Han 2014) on Milky Way spiral arms noticed signatures of kinked spiral arms, segments of which could be fitted with log-periodic spiral functions with different pitch angles. Following such observations, we do not restrict our analysis to perfectly described log-periodic spirals but use the ones that allow for the existence of gaps in the observed spiral arms. Hou (2021) models each of the spiral arms with

[3] https://pypi.org/project/mw-plot/

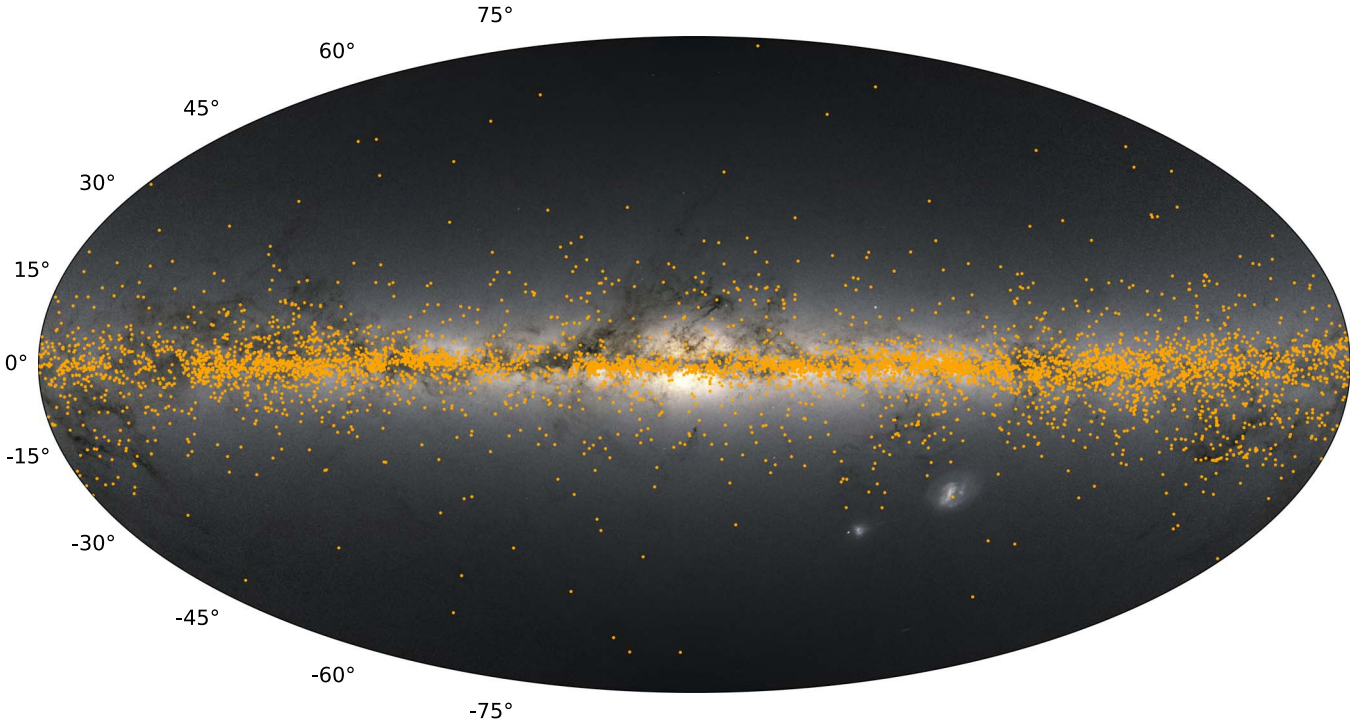

Figure 1. An on-sky view of the Galaxy generated using mw-plot in the Galactic longitude–latitude (l–b) plane juxtaposed with our sample of 6133 OCs. The image in the background is generated by ESA Gaia EDR3 with a resolution of 15.38 lt-yr per pixel.

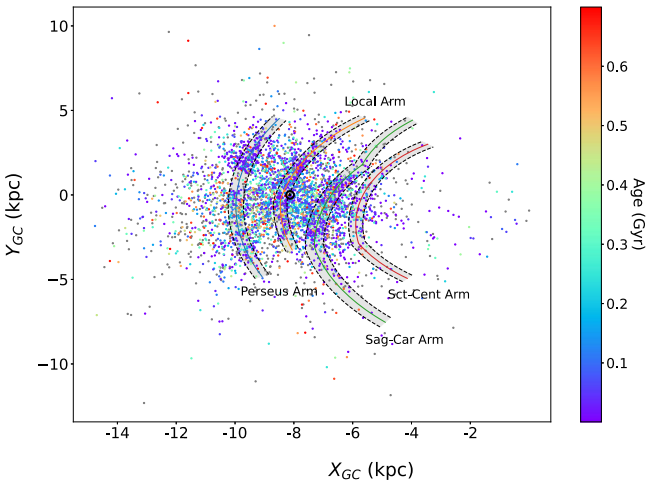

Figure 2. Distribution of the complete sample of OCs in the X–Y plane with the Galactic center at the origin. OCs younger than 700 Myr are color-coded based on their age, while the older ones are shown in gray. The position of the Sun is marked with a black circle at (−8.15, 0) kpc. Spiral arms are taken from Hou (2021).

one kink except the Sagittarius–Carina Arm, which is described using two kinks at $\beta = -22.^{\circ}8$ and $17.^{\circ}5$, respectively. In Figure 2, the regions enclosed within the dashed lines around the spiral arms correspond to the arm widths. The distribution of OCs in spiral arms is not uniform but shows a patchy appearance. It is observed that younger clusters populate the spiral arms while older clusters are mainly present in the interarm regions, as has also been reported in previous studies by Cantat-Gaudin & Anders (2020), Monteiro et al. (2021), Hou (2021), Tarricq et al. (2021), and Poggio et al. (2021).

3.2. Delineation of Spiral Arms

The demarcation of clusters in terms of age band is crucial for untangling the spiral arm structure, as it has been known for a long time that young OCs are ideal tracers of the Galactic spiral arms. In Figure 3, we plot the distribution for three different samples of OCs based on their ages: (i) age/Myr $\leqslant 10$ (top panel), (ii) $10 <$ age/Myr $\leqslant 20$ (middle panel), and (iii) $20 <$ age/Myr $\leqslant 30$ (bottom panel). This displays the respective locations of 501, 355, and 141 OCs in the X–Y plane. The plots depict spiral arms defined by Hou (2021) overplotted as curved solid lines in each of the subplots of Figure 3. The importance of one or more kinks, as also proposed by Reid et al. (2019) and Hou (2021), in the spiral arms becomes apparent in the top panel of Figure 3, especially in the case of the Local and Sagittarius–Carina Arms. The spiral arms deduced by Hou (2021) have allowed us an extended view of the Milky Way spiral arms for a more extensive range of Galactic azimuth in the negative direction than the earlier studies of Reid et al. (2014) and Castro-Ginard et al. (2021). One can observe that the younger OCs (age $<$ 10 Myr) clearly trace out the spiral arms in the solar neighborhood and occupy the regions between spiral arms as they age, while most of the OCs having an age in the range 20–30 Myr are well off from the spiral arms. This means that, in general, most of the OCs leave their birth site after about 10–20 Myr and start populating the interarm regions, where they stay for the rest of their life. Castro-Ginard et al. (2021) has also noted, however, with different age bins, that the OC overdensities showed increased dispersion with time. Moreover, it was also observed that many clusters do not survive longer than about 10–15 Myr after their birth, with the death rate decreasing progressively as they become older and leave the spiral arms (Monteiro et al. 2021).

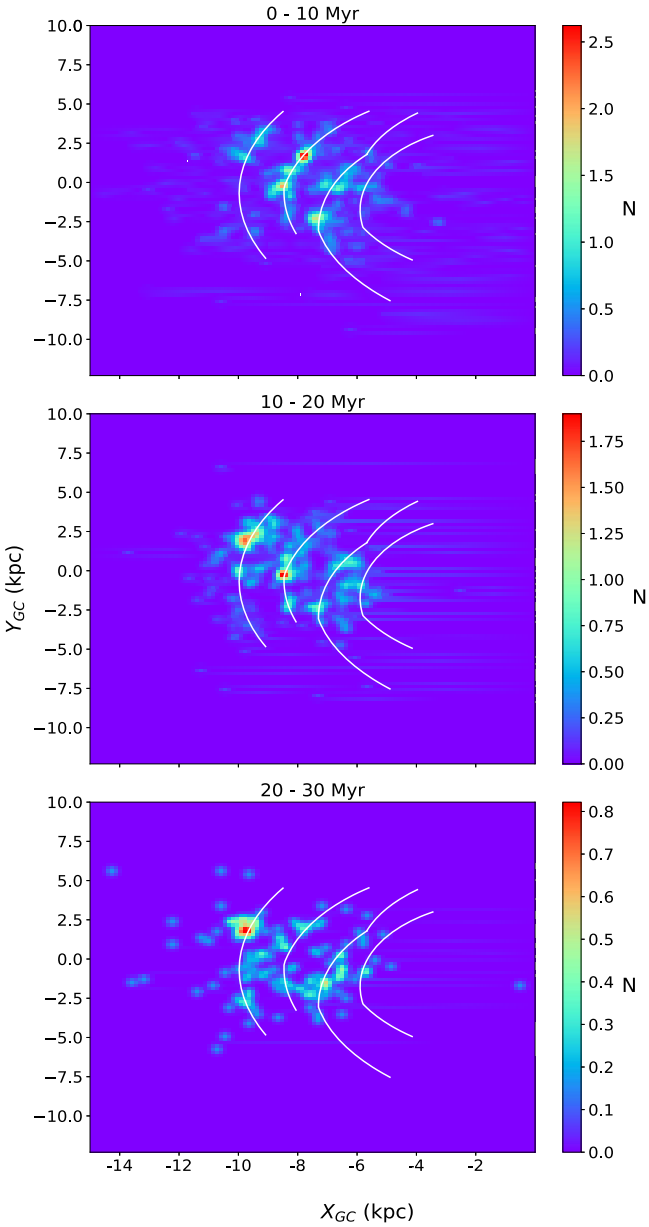

Figure 3. Density heat mapof OCs in different age intervals of $\leqslant$ 10 Myr, 10–20 Myr, and 20–30 Myr (from top to bottom). Spiral arms are traced by the OCs younger than 10 Myr and the older ones occupy the interarm regions. Further, the spiral structure loses its shape in the 20–30 Myr age range.

3.3. Spiral Pattern Rotation Speed

Determining spiral pattern rotation speeds can provide us with critical insights into the nature and evolution of spiral arms. Since the parameters of OCs can be determined with high precision by averaging over their members, one can make use of their kinematic data to estimate the pattern speed of spiral arms (Dias & Lépine 2005; Gerhard 2011). Some recent studies on the determination of spiral pattern rotation speeds include Castro-Ginard et al. (2021), which has made use of 264 young OCs, and Griv et al. (2022), which analyzed 252 OCs within 3 kpc of the Sun and having age $<$ 100 Myr. Taking advantage of a larger sample of OCs available in the present study, we reinvestigated the rotation speeds of spiral arms in the following analysis.

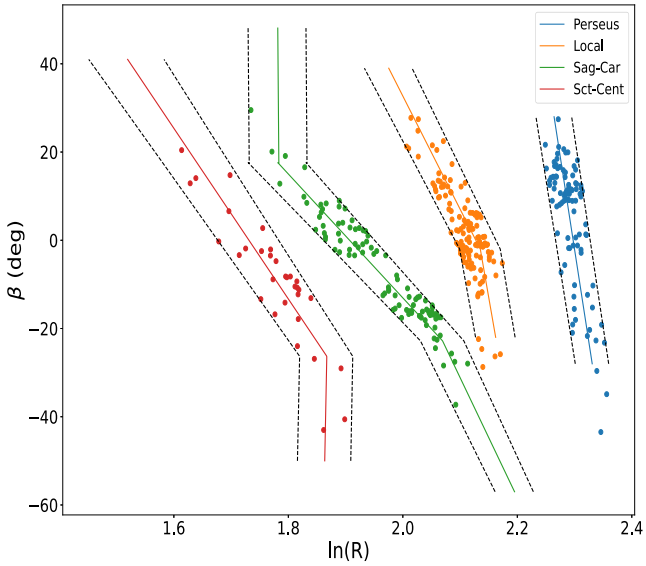

Figure 4. Distribution of OCs in the ln(R)–β plane after arm assignments. The solid lines denote the spiral arms taken from Hou (2021), whereas the dashed lines indicate a width of 0.3 kpc for each spiral arm.

Before proceeding further, we needed to identify the host arms for the OCs. This was done by assigning arms to the OCs lying within 0.3 kpc either side of their nearest arm. Figure 4 shows each arm and the corresponding OCs in the ln(R)–β plane, where R and β are the same as defined in the previous section. The advantage of showing OCs in the ln(R)–β plane is that the spiral arms in this plot can be described with a set of one or more straight lines having different slopes at the positions of kinks, which is helpful in separating the OCs that are currently part of a particular spiral arm. The arm assignment was unambiguous in most cases and was supplemented with the kinematic data of OCs in the case of clusters near the borders. We also included the OCs that were not in the β range of present-day spiral arms but were part of their appropriate extensions, as seen in the case of the Local and the Perseus Arms in the figure. We have taken the solar distance from the Galactic center $R_{\odot}$ as 8.15 kpc and the circular rotation speed at the solar position $\Theta_0 = 236 \pm 7$ km s^{-1} (Reid et al. 2019). We restricted the age of OCs to $\leqslant$ 80 Myr, yielding us a total sample of 371 OCs, of which 93, 148, 98, and 32 OCs are in the Perseus, Local, Sagittarius–Carina (Sag–Car), and Scutum–Centaurus (Sct–Cent) arms, respectively, and also have information available on their radial velocities. As mentioned in Section 2, due to very few OCs with estimated distance uncertainties, we only use the estimated value of the distance for arm assignments of OCs. Therefore, the results of the arm assignments are subject to change in future OC catalogs with slightly different sets of values for the physical parameters of OCs. This reflects on limitation of the inhomogeneous nature of our catalog. However, a relatively small mean uncertainty of 170 pc in distance reported by Dias et al. (2021) using the stellar membership of 1743 OCs determined from Gaia DR2 astrometric data leads us to the conclusion that our subsequent results present an unblemished view of the Milky Way. Figure 5 shows the age distribution of OCs in each arm, where we observe a gradual decline in the number of OCs as the age increases. This might be caused by three factors.

1. With the evolution of clusters in the molecular gas clouds, only about 5% survive by the time they get

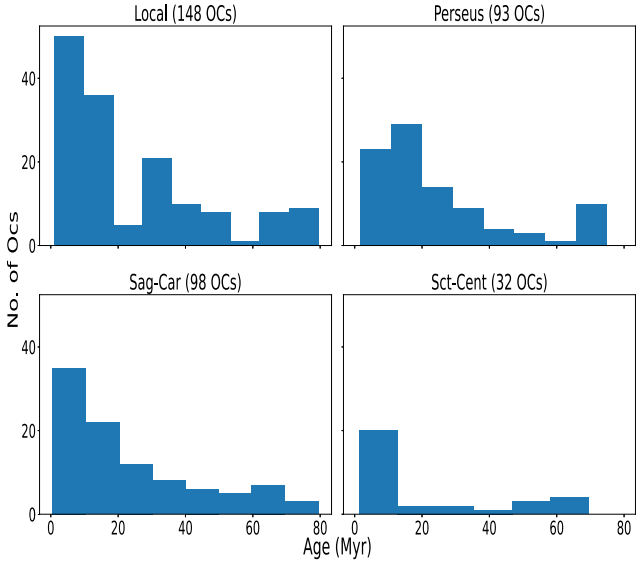

Figure 5. Age distribution of OCs belonging to each spiral arm. The number of clusters assigned to each arm is mentioned in parentheses. As expected, the counts of observed clusters decrease as the age increases.

detached from the parent molecular cloud (Lada & Lada 2003).
2. Older OCs might have undergone disruption due to close encounters with other clusters and clouds of gas.
3. OCs might have moved out of the spiral arms via relative displacement in both the Galactic plane and in a vertical direction away from the Galactic midplane in such a way that they are no longer considered to be a part of the spiral arms (Minchev et al. 2011; Chen & Zhao 2020; Zhang et al. 2021).

Since OCs younger than 10 Myr trace the Milky Way spiral arms quite well and only begin to move away after this time, we used the OCs older than 10 Myr to estimate the rotational speed of the spiral arms. We adopted a similar methodology to that proposed by Dias & Lépine (2005) to compute the pattern speed Ω corresponding to each arm:

1. Arm assignment was done for each OC and each arm was studied separately.
2. Birthplaces were found by integrating the orbit of each OC backward, and it was assumed that these birthplaces represent points on the spiral arm a time T ago, where T denotes the age of each cluster.
3. Once we had the birthplaces of OCs, we assumed that the spiral arms traversed a circular path in the Galactic X–Y plane with time and calculated the present-day Galactic azimuths for a particular pattern speed Ω given the Galactic azimuths corresponding to the birthplaces of OCs. Mathematically,

$$\beta_{\mathrm{G,present}} = \beta_{\mathrm{G,birth}} + \Omega T.$$

4. We estimated the optimal value of Ω by minimizing the distance between the present-day spiral arms and their integrated present-day locations. The mean of the pattern speeds obtained for OCs in a spiral arm was reported as its best value Ω with its dispersion represented by the standard deviation.

We performed the OC orbit integration following the MWPotential2014 of the Python package GALPY (Bovy 2015), which is fit to various observational constraints and is composed of a spherical nucleus and a bulge, a Navarro–Frenk–White dark matter halo, and a Miyamoto–Nagai disk. The numerical integration was done using the Leapfrog integration scheme, where the orbits were traced back in steps of 0.1 Myr. Also, we have rejected data points on the integrated spiral arms that did not lie within 0.3 kpc of the analytical spiral arms; the number of such rejected data points varies when using different values for Ω. Since uncertainty in age is the dominant source of error in the computed birthplaces, we estimated the typical value of the error in age, whenever available, to be about 20%, which is close to the value of 22% average age error for a sample of 581 OCs reported by de la Fuente Marcos & de la Fuente Marcos (2004). Hence, we iterated the above process 100 times by using the age values of clusters with corresponding random errors ranging from 0% to 20%. The mean value and the standard deviation are reported in Table 2 as the optimal value and the corresponding dispersion in the pattern speed Ω.

Table 2
Rotation Speeds of Spiral Arms for Four Different Spiral Arms and Three Different Age Intervals

Arm	No. of OCs	Ω_{rot} (km s^{-1} kpc^{-1})		
		(10–80 Myr)	(10–50 Myr)	(50–80 Myr)
Perseus	93	23.09 ± 0.82	18.97 ± 0.76	25.78 ± 1.13
Local	148	31.47 ± 0.55	32.86 ± 0.64	30.32 ± 1.12
Sag–Car	98	30.9 ± 0.59	29.56 ± 0.94	31.97 ± 1.2
Sct–Cent	32	52.99 ± 2.34	51.99 ± 4.15	53.02 ± 3.54

We computed the pattern speeds of each spiral arm for different age bins to investigate whether the spiral arms have accelerated in the last 80 Myr. The resultant values are given in Table 2, where the rotation speed of each arm is provided in units of km s^{-1} kpc^{-1} along with the number of OCs younger than 80 Myr assigned to each spiral arm. Here, one has to note that the estimated errors in the pattern speeds represent only a lower limit since we could not account for the errors in 3D kinematics and distance measurements due to their unavailability in the reference catalogs. Moreover, Castro-Ginard et al. (2021) performed a simulation that aimed at examining whether the proposed methodology can be used to distinguish two different values of Ω_{rot} (in their case 20 and 50 km s^{-1} kpc^{-1}). As a result, they obtained a typical systematic error of 0.8–6 km s^{-1} kpc^{-1} in the imposed pattern speed and were able to conclude that though the methodology for the determination of spiral arm pattern speed is not accurate enough to estimate the exact pattern speeds of individual spiral arms, it is sufficiently good to be able to differentiate between two very different values of pattern speeds. Keeping the above facts in mind, one can deduce the following arguments from the estimated pattern speeds given in Table 2:

1. On comparing the pattern speeds of a particular spiral arm across different age bins, it is evident that the spiral arms have not accelerated in the last 80 Myr.
2. In a particular age bin, the estimated pattern speeds of the four spiral arms follow a declining trend as a function of Galactocentric radius as seen in Figure 6, except for the case of the Local Arm, which has a slightly higher mean pattern speed than the Sag–Car arm.

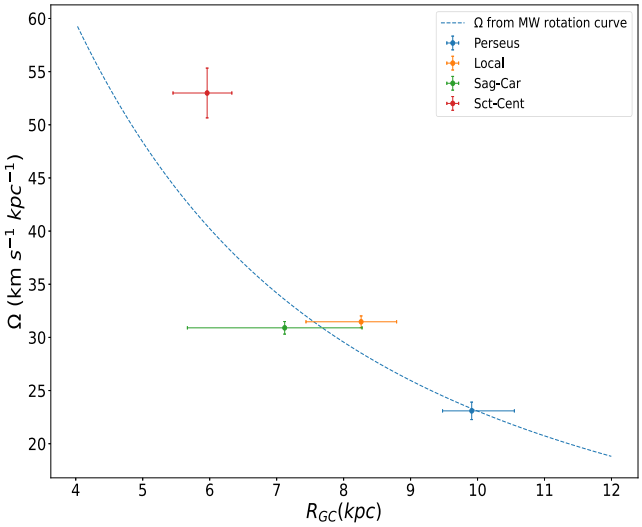

Figure 6. Spiral arm pattern speeds corresponding to the 10–80 Myr interval estimated for the Sct–Cent, Sag–Car, Local, and Perseus Arms shown along with the angular velocity obtained from the MWPotential2014 rotation curve as a function of Galactocentric distance. The R_{GC} values for the solid data points and the associated horizontal error bars denote the mean Galactocentric distance and its spread for the distribution of OCs in each spiral arm, respectively.

3. Though there have been recent indications that the Local arm is larger than previously thought with its pitch angle comparable to those of the Galaxy's other major arms (Xu et al. 2016), this contrasting behavior requires further investigation. A similar observation was also made by Castro-Ginard et al. (2021), though we cannot compare the exact values of the pattern speeds in the two studies due to different values of $R_\odot$ and $V_\odot$ used to normalize the rotation curve.

Our results are in favor of a flocculent Milky Way with short-lived transient spiral arms that corotate with the Milky Way disk at every point (Grand & Kawata 2012; Kawata et al. 2014). This is in substantial agreement with the recent works done by Hunt et al. (2018) and Quillen et al. (2018), who have been able to explain particular ridge and arc-like features in the phase space distributions of stars in the local neighborhood by models of winding spiral arms with different pattern speeds at different Galactocentric radii. However, our results are in stark contrast with the work done by Dias et al. (2019) and Monteiro et al. (2021), who adopt the same methodology and obtain the same pattern speed for all spiral arms while supporting the density wave scenario of the Milky Way spiral arms. Further, several numerical *N*-body simulations (Dobbs & Bonnell 2006; Sellwood 2011; Wada et al. 2011; Pérez-Villegas et al. 2012; Roca-Fàbrega et al. 2013; Michikoshi & Kokubo 2018) lead to a transient behavior of spiral arms corotating with the disk stars in the case of unbarred or weak bar galaxies. Moreover, a lack of an age gradient of clusters across the spiral arms (Dobbs & Pringle 2010; Castro-Ginard et al. 2021) also points in a similar direction.

4. Distribution of OCs Perpendicular to the Galactic Plane

For a symmetric Galaxy, the numbers of OCs below and above the Galactic plane are expected to be the same, and the number density of the OCs is maximum near the Galactic plane and falls steadily as one goes away from the midplane.

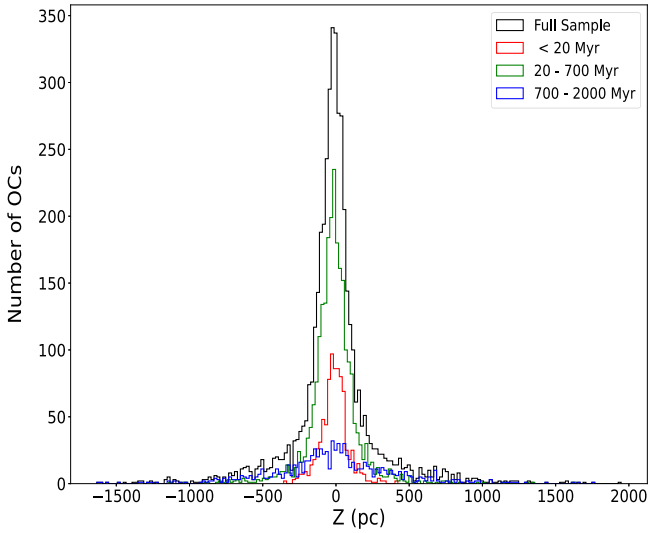

Figure 7. Z distribution of OCs corresponding to different age intervals. The scale height is estimated while assuming a constant solar offset $z_\odot$ of 17.0 ± 0.9 pc for all the plots. The sample is restricted to $(-2, 2)$ kpc in z. The colors corresponding to each OC sample are mentioned in the plot's top right corner.

However, it is known that there is an asymmetry in the distribution of OCs around the Galactic midplane. In Figure 7, which shows the vertical distance distribution ($z = d \sin b$, where d is the heliocentric distance and b is the Galactic latitude), we divided the cluster sample into different bins in z with a bin width of 20 pc, wherein the number distribution peaks at $z \sim -15$ pc. Since there were very few OCs at more considerable vertical distances, we have restricted z to OCs within 2 kpc of the Galactic plane, up to which the sample of OCs is generally complete. This has left us with 4372 OCs used in the following analysis.

4.1. Solar Offset

It is commonly assumed that the distribution of cluster number density perpendicular to the Galactic plane can be well described in the form of an exponential decaying away from the Galactic plane, as given by Chen et al. (1998):

$$N = N_0 \exp\left(-\frac{|z + z_\odot|}{z_h}\right)$$

where $z_\odot$ and z_h are the solar offset and scale height, respectively. Here, N_0 is the maximum cluster density, which by definition is attained at a vertical height $z = -z_\odot$. Knowledge of the exact value of $z_\odot$ is essential not just for the Galactic structure models but also in describing the north–south asymmetry in the density distribution of different kinds of stellar populations in the north and south Galactic regions (Cohen 1995; Chen et al. 1999; Joshi 2005; Bobylev & Bajkova 2016a). However, to accurately determine the solar offset, we must consider the OCs close to the Galactic plane to prevent any bias induced by distant clusters. To do this, we applied the age cutoff for OCs as the clusters start drifting away from the Galactic midplane as they age. We refer the reader to Figure 2 of Joshi (2007), and on using the same methodology, we only considered OCs younger than ∼700 Myr. We determined $z_\odot$ by fitting the above exponential function to

Table 3
Estimated Scale Heights for Different Age Intervals of the Cluster Sample while Keeping the Solar Offset $z_\odot = 17.0 \pm 0.9$ pc Fixed

Age Interval (Myr)	z_h (pc)	No. of OCs
Full sample	100.8 ± 1.7	4372
<20	80.8 ± 8.0	837
<700	91.7 ± 1.9	3376
<2000	98.8 ± 1.6	4107
20–700	96.4 ± 1.9	2439
700–2000	294.7 ± 19.5	831

the sample of OCs younger than 700 Myr and obtained an estimate of $z_\odot = 17.0 \pm 0.9$ pc.

Numerous studies have estimated $z_\odot$ using a wide variety of celestial sources, and most of these studies obtained $z_\odot$ in the range of 10–25 pc to the north of the Galactic plane (e.g., Joshi 2007; Majaess et al. 2009; Buckner & Froebrich 2014; Yao et al. 2017; Siegert 2019; Cantat-Gaudin et al. 2020; Griv et al. 2021). Though a direct comparison of $z_\odot$ in different studies is difficult, it is found that the choice of the data sample and method of determination account for most of the disagreements among $z_\odot$ values (Joshi 2007; Cantat-Gaudin et al. 2020). Reid et al. (2019) attributed these differences as a combination of extinction and Galactic warping. It is observed that $z_\odot$ derived through young tracers such as H II regions, masers, and molecular clouds is generally lower than that found using stellar tracers such as classical Cepheids, RR Lyrae stars, and star clusters (e.g., Bobylev & Bajkova 2016a, 2016b; Karim & Mamajek 2017). Nevertheless, our present estimate of $z_\odot$ is in remarkable agreement with Bobylev & Bajkova (2016a)'s mean value of 16 ± 2 pc and Karim & Mamajek (2017)'s median value of 17 ± 2 pc.

4.2. Cluster Scale Height

The observed clusters distribution perpendicular to the Galactic plane provides us with an estimate of the thickness of the young Galactic disk. We fitted the number distribution of OCs in the exponential profile as described by Equation (1) to estimate the scale height; the best fit for the sample of 4372 OCs resulted in a scale height of $z_h = 100.8 \pm 1.7$ pc. However, the large value of z_h is mainly influenced by the older clusters, which are mostly located at higher latitudes, resulting in a shallower wing in the z distribution. We plot a similar distribution of OCs perpendicular to the Galactic plane but using different age bins: <20 Myr (red), 20–700 Myr (green), and 700–2000 Myr (blue), corresponding to 837, 2439, and 831 OCs respectively. We fitted the exponential profile in all these three samples to estimate the scale height while keeping the solar offset $z_\odot = 17.0$ pc as a fixed value as derived in the previous subsection. In addition, we also determined scale heights for the larger cluster sample having age <700 Myr and <2000 Myr. Table 3 provides information about the scale heights obtained for different age bins and the corresponding number of OCs. The scale height increases as we fit the exponential distribution to older OCs, as is also evident in Figure 7, which is consistent with the hypothesis that OCs migrate toward the outer disk as they age. The pattern speed of spiral arms exhibits a decreasing trend with increasing Galactocentric distance. For a sample of OCs younger than 700 Myr, z_h is obtained as 91.7 ± 1.9 pc. A range of cluster scale heights has been published by the authors in previous studies. For example, Bonatto et al. (2006) derived a scale height of 48 ± 3 pc for OCs younger than 200 Myr; Joshi et al. (2016) obtained $z_h = 64 \pm 2$ pc for OCs within 1.8 kpc of the Sun. Buckner & Froebrich (2014) found the scale height increases from about 40 pc at 1 Myr to 75 pc at the age of 1 Gyr. Some more recent studies, such as Cantat-Gaudin et al. (2020), obtained a scale height of 74 ± 5 pc for OCs in the solar neighborhood with a typical age of ∼100 Myr. Similarly, Hao et al. (2021) reported a scale height of 70.5 ± 2.3 pc for young OCs (age < 20 Myr), which increases to 87.4 ± 3.6 pc for older OCs with ages of 20–100 Myr. Although it is difficult to compare different estimates due to their different sample selection criteria, our present value of $z_h = 91.7 \pm 1.9$ pc for clusters younger than < 700 Myr agrees with most of these recent estimates.

Further, it has also been established that the OCs farther away from the Galactic center are present at higher altitudes from the Galactic plane, hence resulting in the variation of scale height z as a function of the projected Galactocentric distance (R_{GC}). Bonatto et al. (2006) observed that the scale height increases by a factor of two when one compares the two estimates for OCs inside and outside the solar circle. Buckner & Froebrich (2014) and Joshi et al. (2016) showed a positive trend between the Galactocentric distance and the scale height. Using our OC sample, we calculated the scale height (z_h) for two cases: (i) $R_{GC} \leqslant 8.15$ kpc and (ii) $R_{GC} > 8.15$ kpc, comprising 1865 and 2513 OCs respectively. Here, 8.15 kpc is taken as the location of the solar orbit (Reid et al. 2019). We obtained z_h to be 79.2 ± 1.6 pc and 138.1 ± 1.7 pc for the two cases, respectively, which further affirms the dependence of z_h on the Galactocentric distance, in agreement with both these studies.

5. Summary

In this work, we compiled various catalogs of Galactic OCs that became available recently and found a total of 6133 OCs, most of which have been detected in the post-Gaia phase using the photometric and kinematic information provided in the Gaia archive data. Since all open clusters, including the progenitors of giant molecular clouds, are believed to have begun their lives in the Galactic disk, they have been widely used in the study of its structure. We used the position, distance, age, and kinematic parameters of these clusters in the Milky Way to study the Galactic disk morphology. For our work, we rely on the catalogs provided in more than 35 references published in the past. The ages of OCs cover a whole range, from a few million years to tens of billions of years, making them excellent tracers for investigating the Galactic disk, spiral structure, and in particular the evolution of spiral arms. Though our cluster sample seems complete only up to 2 kpc from the Sun, clusters are found to be located as far as 13 kpc from the solar position.

As the young open clusters remain close to their birthplace and, in most cases, are associated with star-forming regions, they make ideal tracers to probe the spiral arms of the Galaxy. The distribution of our sample of OCs in the 2D plane clearly showed signatures of the spiral arms, mainly when we restricted the cluster sample to those younger than 30 Myr, as older OCs have a more scattered distribution. The distributions of OCs reveal the complex substructures in the spiral arms and interarm regions. By analyzing young clusters in different age bins, we could delineate the spiral structures

and found that clusters start leaving the spiral arms after 10–20 Myr and fill the interarm regions, where they stay for the rest of their lives. The distribution of these young clusters traced a four-arm spiral in the Galaxy. The two spiral structures related to the Local and Sagittarius–Carina spiral arms were conspicuous by their presence. In contrast, some substructures of the Perseus and Scutum–Centaurus spiral arms were feebly present. Once we could trace the spiral arms using the younger clusters, we studied their pattern speed by adopting the methodology given by Dias & Lépine (2005). With the help of a large sample of OCs with 3D kinematics, we found that the spiral arms rotate with different individual pattern speeds, which tend to follow a declining trend as one moves to greater Galactocentric radius. This suggests that the Milky Way spiral arms might be transient in nature, thereby favoring a flocculent Milky Way. On comparing the pattern rotation speeds of spiral arms across different age bins, it is found that they have not changed much in the last 80 Myr.

The number density distribution of OCs has been used to determine the Solar offset and scale height, which are about 17.0 ± 0.9 pc and 91.7 ± 1.9 pc, respectively, for clusters younger than 700 Myr. However, we found these numbers vary slightly when we alter the selection criteria of the chosen cluster sample in terms of age, distance perpendicular to the Galactic plane, and Galactocentric distance. In the near future, more improved parallax and distance estimates are expected to be available in the Gaia DR4 survey, providing a larger sample of open clusters having precise physical parameters. This in turn will allow better in-depth study of spiral arm features and constraints on the formation of spiral arms in the Galaxy.

Acknowledgments

We thank referee for suggestions that have improved the quality of this paper. S.M. is grateful to ARIES for providing support through its Visiting Student Program (VSP) to conduct his master's thesis project. We would also like to thank Deepak for his critical remarks. This work has made use of data from the European Space Agency (ESA) mission Gaia (https://www.cosmos.esa.int/gaia), processed by the Gaia Data Processing and Analysis Consortium (DPAC, https://www.cosmos.esa.int/web/gaia/dpac/consortium).

ORCID iDs

Yogesh C. Joshi https://orcid.org/0000-0001-8657-1573
Sagar Malhotra https://orcid.org/0000-0012-3245-1234

References

Bobylev, V. V., & Bajkova, A. T. 2016a, AstL, 42, 1
Bobylev, V. V., & Bajkova, A. T. 2016b, AstL, 42, 182
Bonatto, C., Kerber, L. O., Bica, E., & Santiago, B. X. 2006, A&A, 446, 121
Bossini, D., Vallenari, A., Bragaglia, A., et al. 2019, A&A, 623, A108
Bovy, J. 2015, ApJS, 216, 29
Buckner, A. S. M., & Froebrich, D. 2013, MNRAS, 436, 1465
Buckner, A. S. M., & Froebrich, D. 2014, MNRAS, 444, 290
Cantat-Gaudin, T. 2022, Univ, 8, 111
Cantat-Gaudin, T., & Anders, F. 2020, A&A, 633, A99
Cantat-Gaudin, T., Anders, F., Castro-Ginard, A., et al. 2020, A&A, 640, A1
Cantat-Gaudin, T., Jordi, C., Vallenari, A., Bragaglia, A., et al. 2018, A&A, 618, A93
Cantat-Gaudin, T., Krone-Martins, A., et al. 2019, A&A, 624, A126
Carrera, R., Bragaglia, A., Cantat-Gaudin, T., et al. 2019, A&A, 623, A80
Casamiquela, L., Soubiran, C., Jofré, P., et al. 2021, A&A, 652, A25
Castro-Ginard, A., Jordi, C., Luri, X., et al. 2022, A&A, 661, A118
Castro-Ginard, A., Jordi, C., Luri, X., Cantat-Gaudin, T., & Balaguer-Núñez, L. 2019, A&A, 627, A35
Castro-Ginard, A., McMillan, P. J., Luri, X., Jordi, C., et al. 2021, A&A, 652, A162
Chen, B., Figueras, F., Torra, J., et al. 1999, A&A, 352, 459
Chen, B., Vergely, J. L., Valette, B., & Carraro, G. 1998, A&A, 336, 137
Chen, L., Hou, J. L., & Wang, J. J. 2003, AJ, 125, 1397
Chen, Y. Q., & Zhao, G. 2020, MNRAS, 495, 2673
Chi, H., Wang, F., Wang, W., Deng, H., & Li, Z. 2023, ApJS, 266, 36
Cohen, M. 1995, ApJ, 444, 874
de la Fuente Marcos, R., & de la Fuente Marcos, C. 2004, NewA, 9, 475
Dias, W. S., Alessi, B. S., Moitinho, A., & Lépine, J. R. D. 2002, A&A, 389, 871
Dias, W. S., & Lépine, J. R. D. 2005, ApJ, 629, 825
Dias, W. S., Monteiro, H., Caetano, T. C., et al. 2014, A&A, 564, A79
Dias, W. S., Monteiro, H., Lépine, J. R. D., & Barros, D. A. 2019, MNRAS, 486, 5726
Dias, W. S., Monteiro, H., Moitinho, A., et al. 2021, MNRAS, 504, 356
Díaz-García, S., Salo, H., Knapen, J. H., & Herrera-Endoqui, M. 2019, A&A, 631, A94
Dobbs, C. L., Bending, T. J. R., Pettitt, A. R., Buckner, A. S. M., & Bate, M. R. 2022, MNRAS, 517, 675
Dobbs, C. L., & Bonnell, I. A. 2006, MNRAS, 367, 873
Dobbs, C. L., & Pringle, J. E. 2010, MNRAS, 409, 396
D'Onghia, E., Vogelsberger, M., & Hernquist, L. 2013, ApJ, 766, 34
Donor, J., Frinchaboy, P. M., et al. 2020, AJ, 159, 199
Donor, J., Frinchaboy, P. M., Cunha, K., et al. 2018, AJ, 156, 142
Ferreira, F. A., Corradi, W. J. B., Maia, F. F. S., Angelo, M. S., & Santos, J. F. C. J 2020, MNRAS, 496, 2021
Ferreira, F. A., Santos, J. F. C., Corradi, W. J. B., Maia, F. F. S., & Angelo, M. S. 2019, MNRAS, 483, 5508
Gaia Collaboration, Brown, A. G. A., Vallenari, A., et al. 2016, A&A, 595, A2
Gaia Collaboration, Brown, A. G. A., Vallenari, A., et al. 2018, A&A, 616, A1
Gerhard, O. 2011, MSAIS, 18, 185
Glushkova, E. V., Koposov, S. E., Zolotukhin, I. Y., et al. 2010, AstL, 36, 75
Grand, R. J. J., Kawata, D., & Cropper, M. 2012, MNRAS, 421, 1529
Griv, E., Gedalin, M., & Jiang, I.-G. 2022, MNRAS, 512, 1169
Griv, E., Gedalin, M., Pietrukowicz, P., Majaess, D., & Jiang, I.-G. 2021, MNRAS, 502, 4194
Hao, C. J., Xu, Y., Hou, L. G., et al. 2021, A&A, 652, A102
Hao, C. J., Xu, Y., Wu, Z. Y., et al. 2022a, A&A, 668, A13
Hao, C. J., Xu, Y., Wu, Z. Y., et al. 2022b, A&A, 660, A4
He, Z., Li, C., Zhong, J., et al. 2022a, ApJS, 260, 8
He, Z., Wang, K., Luo, Y., et al. 2022b, ApJS, 262, 7
He, Z.-H., Xu, Y., Hao, C.-J., Wu, Z.-Y., & Li, J.-J. 2021, RAA, 21, 093
Honig, Z. N., & Reid, M. J. 2015, ApJ, 800, 53
Hou, L. G. 2021, FrASS, 8, 103
Hou, L. G., & Han, J. L. 2014, A&A, 569, A125
Hu, Q., Zhang, Y., Esamdin, A., Liu, J., & Zeng, X. 2021, ApJ, 912, 5
Hunt, J. A. S., Hong, J., Bovy, J., Kawata, D., & Grand, R. J. J. 2018, MNRAS, 481, 3794
Joshi, Y. C. 2005, MNRAS, 362, 1259
Joshi, Y. C. 2007, MNRAS, 378, 768
Joshi, Y. C., Dambis, A. K., Pandey, A. K., & Joshi, S. 2016, A&A, 593, A116
Karim, T., & Mamajek, E. E. 2017, MNRAS, 465, 472
Kawata, D., Hunt, J. A. S., Grand, R. J. J., Pasetto, S., & Cropper, M. 2014, MNRAS, 443, 2757
Kendall, S., Kennicutt, R. C., & Clarke, C. 2011, MNRAS, 414, 538
Kharchenko, N. V., Piskunov, A. E., Schilbach, E., Röser, S., & Scholz, R. D. 2013, A&A, 558, A53
Kharchenko, N. V., Scholz, R. D., Piskunov, A. E., Röser, S., & Schilbach, E. 2007, AN, 328, 889
Kounkel, M., Covey, K., & Stassun, K. G. 2020, AJ, 160, 279
Krumholz, M. R., McKee, C. F., & Bland-Hawthorn, J. 2019, ARA&A, 57, 227
Lada, C. J., & Lada, E. A. 2003, ARA&A, 41, 57
Liu, L., & Pang, X. 2019, ApJS, 245, 32
Loktin, A. V., & Beshenov, G. V. 2003, ARep, 47, 6
Majaess, D. J., Turner, D. G., & Lane, D. J. 2009, MNRAS, 398, 263
Mermilliod, J. C., Mayor, M., & Udry, S. 2008, A&A, 485, 303
Michikoshi, S., & Kokubo, E. 2018, MNRAS, 481, 185
Minchev, I., Famaey, B., Combes, F., et al. 2011, A&A, 527, A147
Monteiro, H., Barros, D. A., Dias, W. S., & Lépine, J. R. D. 2021, FrASS, 8, 62
Myers, N., Donor, J., et al. 2022, AJ, 164, 85

Netopil, M., Oralhan, İ. A., Çakmak, H., Michel, R., & Karataş, Y. 2022, MNRAS, 509, 421
Netopil, M., Paunzen, E., Heiter, U., & Soubiran, C. 2016, A&A, 585, A150
Pérez-Villegas, A., Pichardo, B., Moreno, E., Peimbert, A., & Velázquez, H. M. 2012, ApJL, 745, L14
Poggio, E., Drimmel, R., Cantat-Gaudin, T., et al. 2021, A&A, 651, A104
Poovelil, V. J., Zasowski, G., et al. 2020, ApJ, 903, 55
Portegies Zwart, S. F., McMillan, S. L. W., & Gieles, M. 2010, ARA&A, 48, 431
Quillen, A. C., Carrillo, I., Anders, F., et al. 2018, MNRAS, 480, 3132
Reid, M. J., Menten, K. M., et al. 2019, ApJ, 885, 131
Reid, M. J., Menten, K. M., Brunthaler, A., et al. 2014, ApJ, 783, 130
Roca-Fàbrega, S., Valenzuela, O., Figueras, F., et al. 2013, MNRAS, 432, 2878
Ryu, J., & Lee, M. G. 2018, ApJ, 856, 152
Schmeja, S., Kharchenko, N. V., Piskunov, A. E., et al. 2014, A&A, 568, A51
Scholz, R. D., Kharchenko, N. V., Piskunov, A. E., Röser, S., & Schilbach, E. 2015, A&A, 581, A39
Sellwood, J. A. 2011, MNRAS, 410, 1637
Siegert, T. 2019, A&A, 632, L1
Sim, G., Lee, S. H., Ann, H. B., & Kim, S. 2019, JKAS, 52, 145
Spina, L., Ting, Y. S., et al. 2021, MNRAS, 503, 3279
Tarricq, Y., Soubiran, C., et al. 2021, A&A, 647, A19
Tarricq, Y., Soubiran, C., Casamiquela, L., et al. 2022, A&A, 659, A59
Taylor, J. H., & Cordes, J. M. 1993, ApJ, 411, 674
Vande Putte, D., Garnier, T. P., Ferreras, I., Mignani, R. P., & Cropper, M. 2010, MNRAS, 407, 2109
Wada, K., Baba, J., & Saitoh, T. R. 2011, ApJ, 735, 1
Xu, Y., Reid, M., Dame, T., et al. 2016, SciA, 2, e1600878
Yao, J. M., Manchester, R. N., & Wang, N. 2017, MNRAS, 468, 3289
Zhang, H., Chen, Y., & Zhao, G. 2021, ApJ, 919, 52
Zhong, J., Chen, L., Jiang, Y., Qin, S., & Hou, J. 2022, AJ, 164, 54
Zhong, J., Chen, L., Wu, D., et al. 2020, A&A, 640, A127